23. Lewellen TK, Miyaoka RS, Kohlmyer SG, Pollard KR. An XYE acquisition interface for General Electric Starcam Anger cameras. *IEEE MIC Conf Proc* 1991;91CH31005: 1861–1865.
24. Rollo FD, Harris CC. Factors affecting image formation. In: Rolloe FD, ed. *Nuclear medicine physics, instrumentation and agents*. St. Louis: C.V. Mosby Co.; 1977:397.
25. Lewellen TK, Miyaoka RS, Kaplan MS, Kohlmyer SK, Costa WC, Jansen F. Preliminary investigation of coincidence imaging with a standard dual-headed spect system [Abstract]. *J Nucl Med* 1995;36(suppl):175P.
26. Haynor DR, Kaplan MS, Harrison RL, Lewellen TK, Harrison RL. Multiwindow scatter correction techniques in single photon imaging. *Med Phys* 1995;22:2015–2024.

Comparison of Continuous Step-and-Shoot versus Step-and-Shoot Acquisition SPECT

ZongJian Cao, Christophe Maunoury, Charles C. Chen and Lawrence E. Holder
Department of Diagnostic Radiology and the Cancer Center, University of Maryland Medical Center, Baltimore, Maryland

This study compared the quality of SPECT images obtained with step-and-shoot mode (SSM) and continuous step-and-shoot mode (CSSM). **Methods:** Computer simulations of SSM and CSSM were performed with a two-dimensional Shepp-Logan head phantom and a high-resolution parallel-hole collimator. The effects of noise and photon attenuation were examined. **Results:** Without noise and without attenuation, small structures in reconstructed images obtained using fast CSSM (less than 4 sec per view plus the moving time from one view to the next) were slightly blurred and rotated in the opposite direction of detector motion. With both noise and attenuation, these artifacts were not visible, and the image quality obtained from CSSM, especially from fast CSSM, was improved as compared to that resulting from the corresponding SSM due to the increasing number of counts. The improvement of image quality became less significant with increasing acquisition time and in the presence of attenuation. **Conclusion:** For fast SPECT, CSSM provided better image quality than the corresponding SSM, especially when attenuation effects were not present. For relatively long time SPECT without attenuation compensation that is typical for clinical studies, the image quality of CSSM was similar to that of SSM.

Key Words: SPECT; step-and-shoot; continuous acquisition
J Nucl Med 1996; 37:2037–2040

There are three modes of SPECT acquisition: step-and-shoot, continuous and continuous step-and-shoot. In the step-and-shoot mode (SSM), projection data are acquired only when the detector is stationary at sequential views. In the continuous mode (CM), data are acquired as the detector moves continuously. In the continuous step-and-shoot mode (CSSM), data are acquired both when the detector is stationary and when the detector moves from one view to the next. Bieszk and Hawman compared CM and SSM using simulation with an ideal pencil-beam collimator and using phantom studies with an ultra-high resolution collimator. They suggested that CSSM might have the sensitivity of CM, but with resolution approaching that of SSM (*1*). A clinical application of CSSM has also been reported (*2*). The purpose of our study was to compare the image quality and identify the strengths and weaknesses of CSSM versus SSM.

MATERIALS AND METHODS

The two-dimensional Shepp-Logan head phantom (*3*) used in this study was composed of six elliptical structures with different positions, orientations, sizes and activities (Table 1). To isolate the effects of detector motion in CSSM, statistical noise and photon attenuation, simulations were performed without noise and without attenuation, with noise and without attenuation, and with noise and with attenuation. A high-resolution collimator was used in the simulations. The data were acquired with 64 views over 360° and with an array of 64 pixels at each view. The time needed to move the detector from one view to the next was set to 4 sec which is typical for most commercial SPECT systems. For SSM, the acquisition times were chosen to be 25, 15, 4 and 1 sec per view. For CSSM, the acquisition time was equal to the SSM time-per-view plus the moving time of the detector, so the corresponding acquisition times were 25 + 4, 15 + 4, 4 + 4 and 1 + 4 sec, respectively.

To simulate continuous acquisition between two adjacent views, the angle between the two views was divided into a number of intervals. The detector stopped and acquired data at the center of each interval. The discrete acquisition mode becomes more continuous with increasing number of intervals. In this study, 8, 16 and 24 intervals were tried for 1 + 4-sec CSSM, and little difference was found among the images visually and quantitatively. Therefore, eight intervals were used to decrease processing time. The projection data were acquired at the midpoint of each interval (the dots in Fig. 1) for 0.5 sec. The angular positions of these midpoints were

$$\varphi_i + \frac{5.625°}{16}, \varphi_i + \frac{5.625° \cdot 3}{16}, \ldots, \text{and } \varphi_i + \frac{5.625° \cdot 15}{16},$$

where φ_i and φ_{i+1} were the angular positions of two adjacent views and the angle between φ_i and φ_{i+1} was 5.625° (=360°/64 views).

TABLE 1
Geometric Parameters Used for the Ellipses in the Two-Dimensional Shepp-Logan-Head Phantom

Ellipse	Semiaxes a and b (cm)	Position of center x and y (cm)	Vertical angle* (°)	Activity weight† (1/cm)
1	a = 11.56, b = 14.75	x = 0, y = 0	0	2
2	a = 11.00, b = 14.12	x = 0, y = 0.25	0	−1
3	a = 2.69, b = 6.12	x = −3.56, y = 0	−18	−1
4	a = 2.12, b = 4.75	x = 3.56, y = 0	18	−1
5	a = 3.75, b = 4.06	x = 0, y = 7.5	0	1
6	a = 0.62, b = 0.62	x = 0, y = −8.75	0	2

*The vertical angle is defined as the angle between the vertical direction and the long axis of an ellipse.

†The activity weight of Ellipse 2 is relative to that of Ellipse 1 and the activity weights of Ellipses 3, 4, 5 and 6 are relative to that of Ellipse 2. For example, the activity of Ellipse 2 is 1 (=2 − 1) and the activity of Ellipse 3 is 0 (=1 − 1). The expression is mathematically convenient for computing the sum of activity along an intersecting ray.

Received July 24, 1995; revision accepted Oct. 18, 1995.
For correspondence or reprints contact: ZongJian Cao, PhD, Department of Radiology, University of Maryland Medical Center, 22 South Greene St., Baltimore, MD 21201.

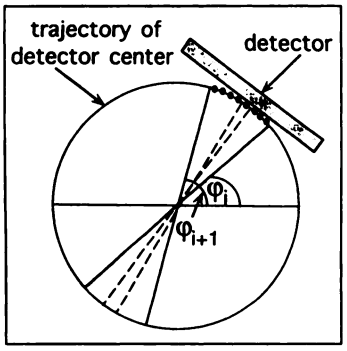

FIGURE 1. Detection geometry of continuous step-and-shoot mode acquisition. Projection data are acquired at each of the eight points between two adjacent views φ_i and φ_{i+1}, and then are added to the data acquired at φ_i.

The data acquired at these eight points were added to the data acquired at view φ_i to form the total data of view φ_i (*2*).

A previously developed analytical approach (*4*) was used to generate noise-free projection data. This method is more efficient computationally than Monte Carlo simulation (*5*) and can be applied to phantoms with regular shapes and uniform attenuation. In generating the data, the intersecting length of a projection ray within an elliptical object in the phantom was obtained by solving the equations of the projection ray and the ellipse. The ray length was used to determine two factors, the contribution of activity from the elliptical objects and the attenuation along the path towards the detector. Then the projection data were determined by these two factors.

Poisson noise was added to the noise-free data (*6*). The noise level was determined by the counts of the data. The number of counts for SSM with 64 views and 25 sec per view was set to 150,000 to simulate a typical clinical image. The corresponding number of counts for CSSM was 174,000. Similarly, a 15-sec per view SSM acquired 90,000 counts and the corresponding CSSM had 114,000 counts. A 4-sec per view acquisition had 24,000 counts for SSM and 48,000 counts for CSSM. A 1-sec acquisition had 6,000 counts for SSM and 30,000 counts for CSSM.

To evaluate the attenuation effect as an isolated factor, we simulated the data with and without attenuation. In the simulations with attenuation, the water attenuation coefficient (0.15/cm) was uniformly assigned to the inside of the phantom.

A parallel-hole collimator allows detection of some oblique projection rays restricted by the acceptance angle of the collimator. The acceptance angle was set to 2.7° that is representative of most commercially available high-resolution parallel-beam collimators.

Reconstructed images of 64 × 64 pixels were obtained using the filtered backprojection algorithm with a ramp filter. Attenuation compensation was not performed since most often it was not used in clinical studies. For noisy images, a fourth-order Butterworth filters with different cut-off frequencies was used. The cut-off frequency depended on the noise level of the image. They ranged from 0.13 to 0.3 cycle per pixel. Intensity profiles and mean squared deviations were used to assess image quality. The mean squared deviation (MSD) was defined as

TABLE 2
Mean-Squared Deviations of the Marked ROIs for Noisy Images without Attenuation

Acquisition mode	ROI I	ROI II	ROI III
SSM 25 s/view	8.25	2.57	1.24
CSSM (25 + 4) s/view	6.49	1.97	0.98
SSM 1 s/view	21.68	5.71	5.99
CSSM (1 + 4) s/view	11.39	2.65	2.40

$$MSD = \frac{1}{N}\sum_{i=1}^{N}(p_i - P)^2,$$

where N was the total number of pixels within a region of interest (ROI), p_i was the pixel value of the ith pixel in the ROI, and P was the true pixel value. For a uniform ROI, P was a constant. Larger MSD represented a greater deviation of the pixel values from the true value, and indicated poorer image quality. Three ROI with the same area (8 × 10 pixels, so N = 80) were chosen at different locations as illustrated in Table 2. The first ROI was located deep inside the phantom, the second ROI was located near the edge of the phantom, and the third ROI was outside the phantom. The true pixel values, P, were 14.20 for the first ROI, 7.10 for the second ROI and 0 for the third ROI.

RESULTS

Simulation Without Noise and Without Attenuation

There were no appreciable differences between the image obtained using SSM (Fig. 2A) and the images obtained using 25 + 4- and 15 + 4-sec CSSM (Fig. 2B, C). However, with 4 + 4- and 1 + 4-sec CSSM, the small bright circle located at the bottom was progressively less well defined (Fig. 2D, E). In addition, the images were rotated slightly in the opposite direction of detector motion, resulting in a shift of the small circle. The center of the small circle represented by the peak of the profile in Figure 3 was shifted about 1 pixel (6.4 mm) towards the left side for 1 + 4 CSSM compared to SSM. The center was progressively less shifted with longer acquisition time.

Simulation With Noise and Without Attenuation

There were no appreciable differences between the 25-sec SSM image and the 25 + 4-sec CSSM image, either without filtering (Fig. 4A, C) or with Butterworth filtering (Fig. 4B, D). However, the image quality obtained using 4 + 4- and 1 + 4-sec CSSM was improved compared to 4- and 1-sec SSM, respectively. The reconstructed images from 1-sec SSM and 1 + 4-sec CSSM were shown in Figure 5. In Table 2, the MSD obtained from 25 + 4-sec CSSM were approximately 80% of the corresponding MSD obtained from 25-sec SSM, while the MSD obtained from 1 + 4 CSSM were 50% of the corresponding MSD obtained from 1-sec SSM.

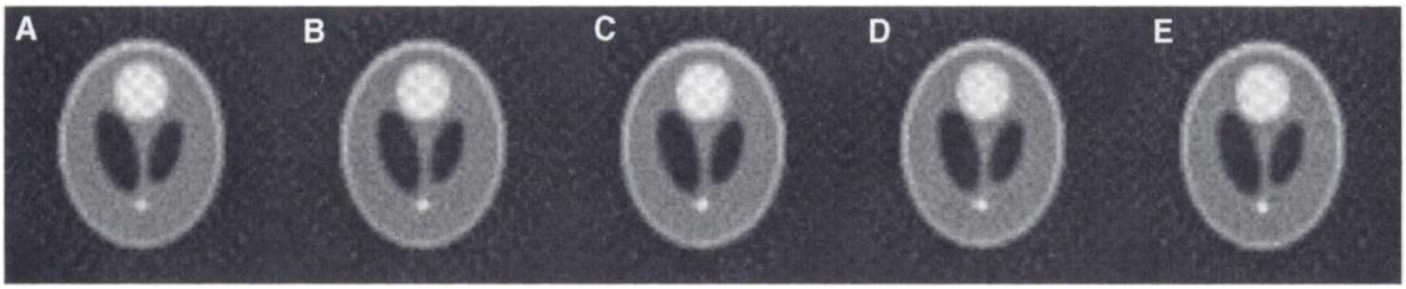

FIGURE 2. Reconstructed images obtained without noise and without attenuation from: (A) SSM, (B) 25 + 4-sec CSSM, (C) 15 + 4-sec CSSM, (D) 4 + 4-sec CSSM and (E) 1 + 4-sec CSSM.

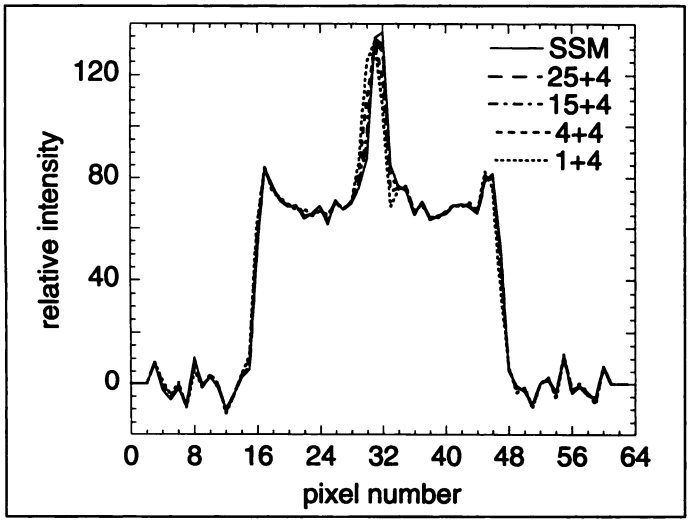

FIGURE 3. Intensity profiles along the marked line of the images in Figure 2A–E.

Simulation With Noise and With Attenuation

With the addition of attenuation, the images appeared darker towards the center and brighter towards the edges of the phantom (Figs. 6, 7) because the photons emitted from the center were more likely absorbed. In the darker central region, the contrast became worse compared to that obtained without attenuation (Figs. 4, 5). The image with attenuation obtained from a 25-sec SSM was similar to the image obtained from 25 + 4-sec CSSM (Fig. 6). However, using 4 + 4- and 1 + 4-sec CSSM, image quality was improved compared to the 4- and 1-sec SSM. The images obtained from a 1-sec SSM and a 1 + 4-sec CSSM were shown in Figure 7. The MSD obtained from a 25 + 4-sec CSSM were about the same as the MSD obtained from a 25-sec SSM, while the MSD obtained from a 1 + 4-sec CSSM were 75–80% of the MSD obtained from a 1-sec SSM (Table 3).

TABLE 3
Mean-Squared Deviations of the Marked ROIs for Noisy Images with Attenuation

Acquisition mode	ROI I	ROI II	ROI III
SSM 25 s/view	41.59	6.98	1.30
CSSM (25 + 4) s/view	39.59	6.96	1.01
SSM 1 s/view	51.36	12.30	4.51
CSSM (1 + 4) s/view	40.91	9.15	3.50

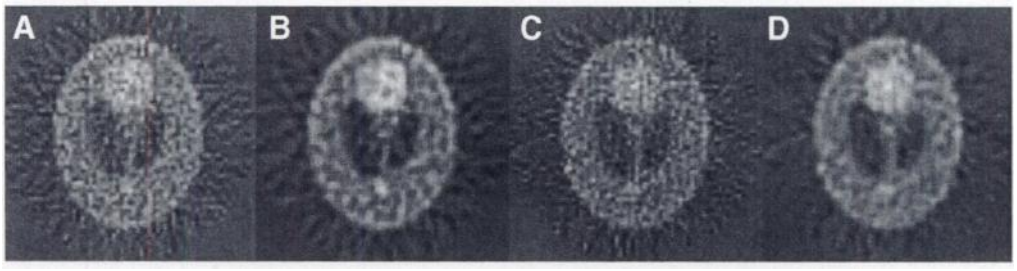

FIGURE 4. Reconstructed images obtained with noise but without attenuation from (A) 25-sec SSM, (B) image A filtered using a fourth-order Butterworth filter with a cutoff frequency of 0.3/pixel, (C) 25 + 4-sec CSSM and (D) image C filtered using the same Butterworth filter.

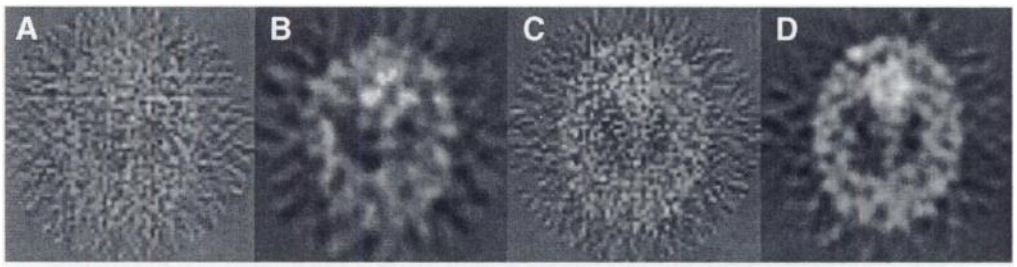

FIGURE 5. Reconstructed images obtained with noise but without attenuation from (A) 1-sec SSM, (B) image A filtered using a fourth-order Butterworth filter with a cutoff frequency of 0.15/pixel, (C) 1 + 4-sec CSSM and (D) image C filtered with a cut off frequency of 0.2/pixel.

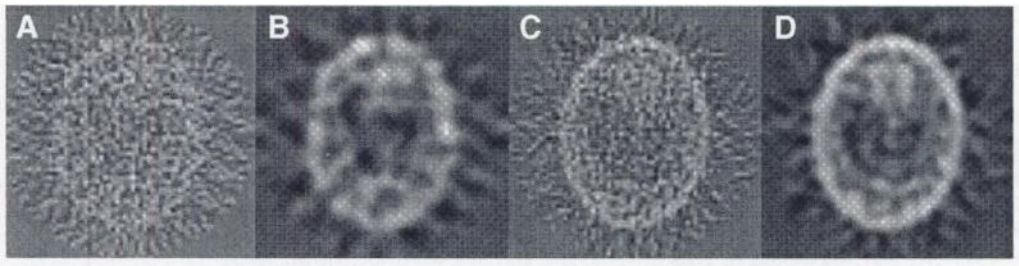

FIGURE 6. Reconstructed images obtained with noise and with attenuation from: (A) 25-sec SSM, (B) image A filtered using a fourth-order Butterworth filter with a cutoff frequency of 0.28/pixel, (C) 25 + 4-sec CSSM and (D) image C filtered using the same Butterworth filter.

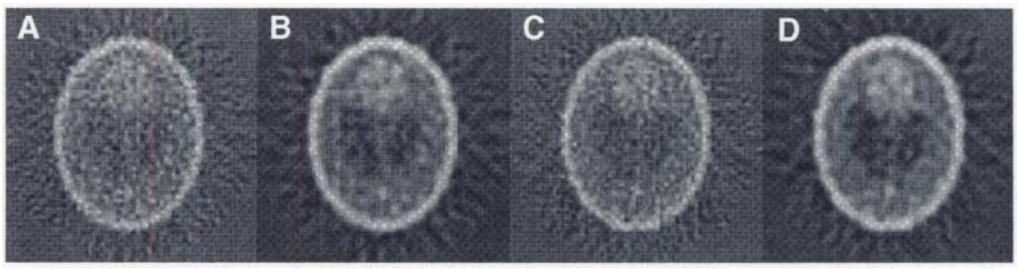

FIGURE 7. Reconstructed images obtained with noise and with attenuation from: (A) 1-sec SSM, (B) image A filtered using a fourth-order Butterworth filter with a cutoff frequency of 0.13/pixel, (C) 1 + 4-sec CSSM and (D) image C filtered with a cutoff frequency of 0.18/pixel.

DISCUSSION

The simulations without noise and without attenuation were designed to illustrate the effects of detector motion between two adjacent views in CSSM. The artifacts were clearly seen in Figures 2 and 3, particularly for the 4 + 4- and 1 + 4-sec CSSM acquisitions that were arbitrarily defined as fast CSSM acquisition because a 64-view study with a dual-head SPECT system could be finished in less than 4 min. The motion artifacts will be reduced by using more than 64 views due to a smaller angular step. In simulations with noise, the relatively minor artifacts of detector motion were covered by the fluctuation of the counts. By separate simulations, we isolated the effect of each of the different factors.

The quality of a noisy image largely depends on the number of counts of projection data. More counts reduce noise and hence improve image quality. A CSSM acquisition provides more counts than the corresponding SSM due to extra data collected as the detector moved from one view to the next. Therefore, the image quality of CSSM, especially fast CSSM, is better than that of the corresponding SSM because of more counts acquired in CSSM. With longer acquisition times (25 + 4 and 15 + 4 sec per view) that are most often used in current clinical studies, the image quality of CSSM is marginally better than that of the corresponding SSM since the total counts are comparable.

With attenuation, image quality obtained from both CSSM and SSM is further degraded. Due to the quality degradation, the improvement in image quality resulting from CSSM became less significant as compared to that obtained without attenuation. Therefore, to take full advantage of CSSM, attenuation effects should be corrected.

CONCLUSION

Image quality obtained from CSSM was appreciably improved compared to that obtained from SSM in fast or dynamic SPECT due to higher counts, but was only marginally better for relatively long-time SPECT due to comparable counts. Improvement in image quality due to CSSM was most noticeable when the attenuation effects were not present. Therefore, attenuation compensation should be performed in image reconstruction of fast SPECT. The results encourage us to conduct phantom and patient studies with CSSM acquisition in the near future.

ACKNOWLEDGMENT

This work was supported in part by U.S. Public Health Grant R29 CA61039 from the National Cancer Institute. Its contents are solely the responsibility of the authors and do not necessarily represent the official views of the National Cancer Institute.

REFERENCES

1. Bieszk JA, Hawman EG. Evaluation of SPECT angular sampling effects; continuous versus step-and-shoot acquisition. *J Nucl Med* 1987;28:1308–1314.
2. Serafini AN, Topchik S, Jimenez H, et al. Clinical comparison of technetium-99m-teboroxime and thallium-201 utilizing a continuous SPECT imaging protocol. *J Nucl Med* 1992;33:1304–1311.
3. Shepp LA, Logan BF. The Fourier reconstruction of a head section. *IEEE Trans Nucl Sci* 1974;21:21–43.
4. Cao ZJ, Tsui BMW. A fully three-dimensional reconstruction algorithm with a nonstationary filter for improved single-orbit cone beam SPECT. *IEEE Trans Nucl Sci* 1993;40:280–287.
5. Ljunberg M, Strand SE. A Monte Carlo program simulating scintillation camera imaging. *Comp Meth Progr Biomed* 1989;29:257–272.
6. Press WH, Flannery BP, Teukolsky SA, Vetterling WT. Numerical recipes. New York, NY: Cambridge University Press; 1986;206–208.

Nonstationary Scatter Subtraction-Restoration in High-Resolution PET

M. Bentourkia, P. Msaki, J. Cadorette and R. Lecomte

Department of Nuclear Medicine and Radiobiology, University of Sherbrooke, Sherbrooke, Québec, Canada

Although removal of object scatter has been shown to improve both contrast and quantitation accuracy, subtraction of detector scatter leads to marginal contrast enhancement and negligible resolution recovery at the expense of reduced sensitivity and increased statistical noise. Since detector scatter has correct information about radioactivity but slightly erroneous information about source location, we suggest that this component should be restored to preserve sensitivity and improve resolution. **Methods:** A scatter correction model that consecutively removes object scatter and restores detector scatter is proposed. The scatter components are processed in the spatial domain using nonstationary scatter kernels. The detector scatter restoration kernel is obtained by piecewise inversion in the Fourier space. The model was tested using line source and hot spot phantom measurements. **Results:** Object scatter subtraction increased contrast substantively with no effect on resolution. Detector scatter restoration recovered resolution almost completely with modest contrast enhancement in small lesions. Spillover effects were reduced to less than 5% for hot spots ≥3 × FWHM, at the expense of moderate noise amplification. **Conclusion:** While subtraction of object scatter is necessary for contrast enhancement and quantitation accuracy, restoration of detector scatter preserves sensitivity and improves quantitation accuracy by reducing spillover effects in high-resolution PET.

Key Words: PET; scatter components; scatter correction; subtraction-restoration; nonstationary

J Nucl Med 1996; 37:2040–2046

Image quality in PET is degraded, among other factors, by scatter contamination from the object, partial volume effects and noise due to low counting statistics. There have been two approaches to minimize these effects in conventional PET systems. In the first method, the effects of scatter are reduced by direct subtraction using integral transformation of the projections with scatter functions characteristic of the imaging system (*1–4*). Since the scatter distributions estimated by this method are fairly smooth, the process does not add significantly to the noise and a low-pass filter to suppress noise is often not

Received June 14, 1995; revision accepted Jan. 28, 1996.

For correspondence or reprints contact: Roger Lecomte, PhD, Department of Nuclear Medicine and Radiobiology, University of Sherbrooke, Sherbrooke, Québec, Canada J1H 5N4.